Russian Journal of Electrochemistry, Vol. 38, No. 3, 2002, pp. 238–246. From Elektrokhimiya, Vol. 38, No. 3, 2002, pp. 274–283.

Simple Analytical Model Predicting Some Features of the Electrolytic Steel-Pickling Process*

N. Ipek[1], N. Lior[2], F. Bark[1], A. Eklund[3], and A. Alemany[4]

[1]*FaxénLaboratoriet, Kungl Tekniska Högskolan, S-100 44 Stockholm, Sweden*

[2]*University of Pennsylvania, Department of Mechanical Engineering and Applied Mechanics, Philadelphia, PA 19104-6315, USA*

[3]*Avesta Sheffield AB, S-774 80 Avesta, Sweden*

[4]*Université Joseph Fourier Laboratoire des Ecoulements Géophysique, Institut de Mécanique de Grenoble, B.P. 53 X-38041 Grenoble, France*

Received March 19, 2001

Abstract—Electrolytic pickling of steel with neutral solutions, to remove the surface scale, reduces the need for the use of strong acids as needed in conventional pickling. This study is a step towards a more in-depth understanding of the factors affecting the former process. A theoretical model, sufficiently simplified to allow analytical solution, is developed and evaluated to provide a first approximation of the potential and current distributions in the electrolyte and steel band. To gain knowledge and validate the model, a small electrolytic pickling cell is constructed, and experiments, including bubble generation and motion observation, are conducted. The experimental work has shown the remarkable bubble production and adherence to the surfaces, and its effects on reducing pickling efficiency and uniformity. The pickling efficiency is about 30%, confirming other researchers' results. The analytical model shows trends very similar to those observed in the experiments, and provides very valuable guidance. It shows, for example, that the current efficiency decreases as the electrode–band distance increases, and it increases with the band thickness and the band-to-electrolyte conductivity ratio. The energy efficiency decreases by orders of magnitude faster than the current efficiency with all of the above-mentioned parameters, because of the correspondingly strong drop in the band–surface potential. A large amount of current is lost due to interelectrode short circuiting.

INTRODUCTION

There is an increasing demand in the steel industry to produce stainless steel at higher rates as well as at lower capital and operating costs. This means that the time to remove the surface oxide layer formed during previous steps of the steel making process has to be shortened, and the pickling process has to be made more efficient. Electrolytic pickling is a method developed to reduce the use of strong acids in this process, and successfully implemented by some steel makers. In this de-scaling method, electrolytic action is used with a neutral aqueous solution of sodium sulfate which forms easy to remove metal sulfates to instead of metal fluorides [1–4].

Considering that existing electrolytic pickling processes are only 30% energy efficient [5], and that it is highly desirable to increase the process throughput and reduce the capital costs, this project to improve the fundamental understanding of the electrolytic pickling process was initiated by Avesta Sheffield AB at the FaxénLaboratoriet of Kungl Tekniska Hogskolan. The problem studied is briefly described as follows. A stainless steel band oxidized on its surfaces is located between electrodes between which an electrical potential difference is imposed. The electrodes and the band are immersed in an aqueous electrolyte. This potential generates an electric current which flows through the electrolyte and the band. Electrolysis of water accompanies the current passage, generating hydrogen or oxygen gas bubbles on different parts of the conducting surfaces. The electrolysis has several important effects on the process: it robs some of the invested electrical energy, and the bubbles have some positive effect in promoting mixing of the electrolyte, and thus the rates of transport for oxide layer removal, but they also have an undesirable effect because they increase the resistance of the electrolyte and thus diminish the current imposed onto the band. Flow in the electrolyte also takes place due to the motion of the steel band and recirculation of the electrolyte for the removal of precipitate and sludge.

As a first approach towards understanding the electrolytic process, a mathematical model was developed based on several simplifying assumptions. The model can be evaluated analytically and thus allow easy fundamental insight into the process by an examination of the potential and current distribution in the electrolytic pickling cell and their sensitivity to the geometric configuration and electrolyte and band conductivities.

*This article was submitted by the authors in English.

1023-1935/02/3803-0238$27.00 © 2002 MAIK “Nauka / Interperiodica”

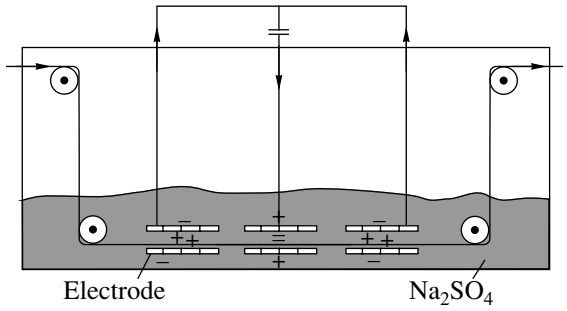

Fig. 1. Electrolytic pickling tank with four-cathode-set at each end and four-anode-set in the center, symmetrically placed above and below a moving steel band; there are four such electrode assemblies in a typical tank.

To learn about the process and validate the modeling, an experimental cell for pickling a stationary steel band was built, and electrolytic pickling experiments were conducted.

FORMULATION OF THE PROBLEM

The Geometry

Studying the configuration of the electrodes in the pickling tank at Avesta Sheffield AB, we found that symmetry prevails in both the horizontal and vertical directions. Therefore we need only take into consideration one electrode set in the modeling.

In the electrolytic pickling tank a group of anodes is arranged after each group of cathodes and the steel band is thereby polarized, cathodically opposite to the anodes and anodically opposite to the cathodes. Throughout the bath there are a total of four electrode sets, where each set, illustrated in Fig. 1, contains four cathodes at the start, four cathodes at the end, and four anodes in the center placed both above and below the steel band. The band acts therefore as an anode, where the actual pickling takes place, twice during each electrode set [6].

As explained in Introduction, the aim of the model presented here is to study the potential and current distributions in the electrolytic cell. Further development of the model would include the chemical reactions, the motion of the steel band, and the electrolytic generation and flow of the bubbles, solvable only by numerical analysis. The modeled geometry, illustrated in Fig. 2, is based on the cell built and used for the pickling experiments (Fig. 3). In the model the electrodes are at a distance H from the steel band center-line. An electrolyte of conductivity κ_e fills the space $(H - D)$ above and beneath the steel band. The steel band thickness is $2D$, length L, and conductivity κ_b.

The Mathematical Model

To represent the alternating polarities of the electrodes in the horizontal direction by a simple mathematical expression, the imposed electrode voltage was assumed to be represented by a sine wave function

$$\Phi_e(X, H) = \Phi_A \sin(KX), \quad (1.1)$$

where Φ_e is the potential in the electrolyte, Φ_A is the electrode voltage amplitude, and K is the wave number of the sine function defined as

$$K \equiv \frac{2\pi n}{L}, \quad (1.2)$$

where n is the number of full sine waves occupying the band length, L. We assume a steady-state two-dimensional problem in Cartesian coordinates with a stagnant electrolyte. The electrical potentials, Φ_e and Φ_b in the electrolyte and steel band, respectively, satisfy the Laplace equation. In the electrolyte,

$$\nabla^2\Phi_e(X, Y) = 0, \quad 0 \le X \le L, \quad D \le Y \le H, \quad (1.3)$$

and in the steel band,

$$\nabla^2\Phi_b(X, Y) = 0, \quad 0 \le X \le L, \quad 0 \le Y \le D. \quad (1.4)$$

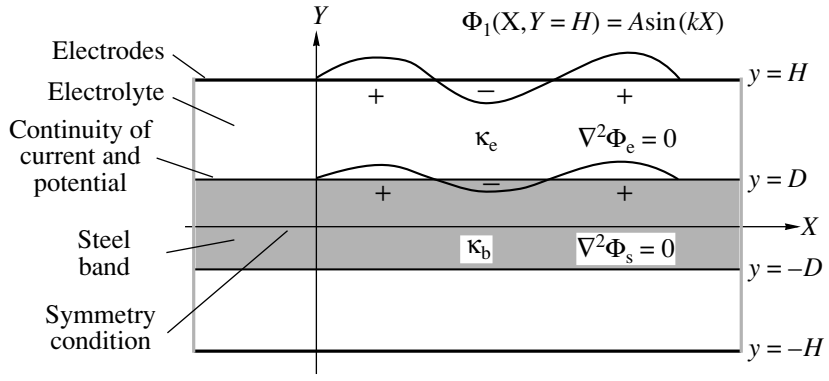

Fig. 2. Model geometry showing the sine wave potential representing two cathodes and anode between them, steel band and potential imposed on it by the electrodes, electrolyte between them, and boundary conditions; L = 300 mm, H = 30 mm, D = 1.5 mm; 170 g l^{-1} electrolyte, κ_e = 9.87 S m^{-1}, $\kappa_b = 10^7$ S m^{-1}.

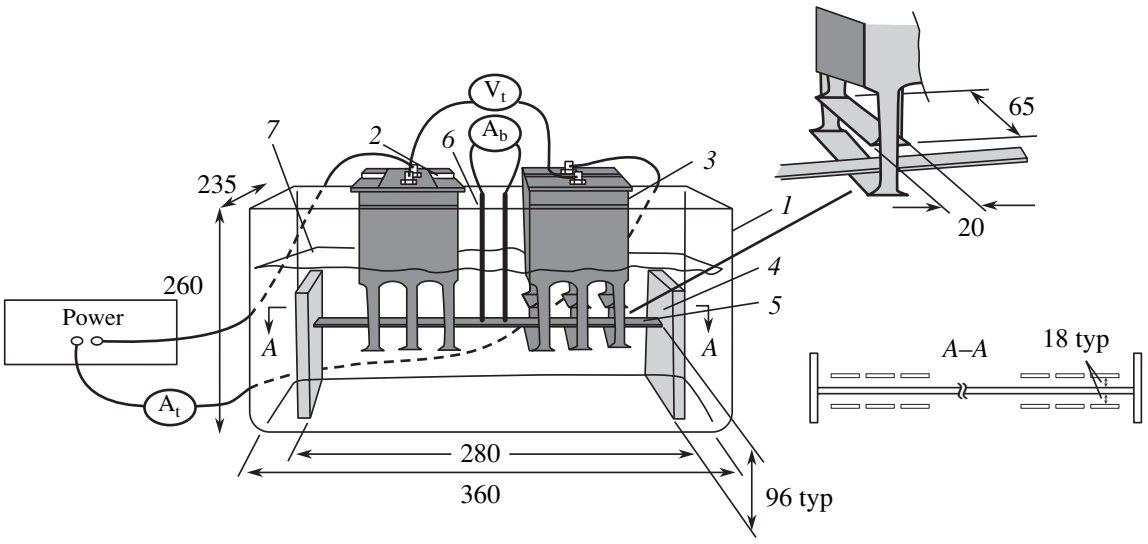

Fig. 3. Experimental cell: (*1*) glass container 360 × 260 × 235 mm; (*2*) lead anodes 20 × 65 mm top, 20 × 85 mm bottom; (*3*) lead cathodes, same size as anodes; (*4*) insulating plastic supports; (*5*) steel band; (*6*) current measuring extension steel rods of stainless steel 304; and (*7*) Na_2SO_4 electrolyte. Magnified details in the upper right corner show two views of the electrode-to-band arrangement and distance (in mm). Voltmeter V_t measures the electrode potential. Ampere meters A_t and A_b measure, respectively, total current and current passing through the steel band.

The boundary conditions at the electrode surface are the imposed potential as stated in Eqs. (1.1) and (1.2), at the interface between the steel band surface and the electrolyte we prescribe potential and current continuity

$$\Phi_e(X, D) = \Phi_b(X, D), \tag{1.5}$$

$$\left[\kappa_e \frac{\partial \Phi_e}{\partial Y}\right]_{X, Y = D} = \left[\kappa_b \frac{\partial \Phi_b}{\partial Y}\right]_{X, Y = D}. \tag{1.6}$$

Only the upper half of the cell is modeled due to symmetry, and at the steel band center-line we apply the symmetry condition

$$\left[\frac{\partial \Phi_b}{\partial Y}\right]_{X, Y = 0} = 0. \tag{1.7}$$

The current densities in the electrolyte, I_e (A m^{-2}), and steel band, I_b (A m^{-2}), are

$$\bar{I}_e = -\kappa_e \nabla \Phi_e, \tag{1.8}$$

$$\bar{I}_b = -\kappa_b \nabla \Phi_b. \tag{1.9}$$

To formulate a dimensionless problem, the variables are scaled as

$$x = \frac{X}{H}, \quad y = \frac{Y}{H},$$
$$\phi_{e, b} = \frac{\Phi_{e, b}}{\Phi_A}, \quad i_{e, b} = \frac{H I_{e, b}}{\kappa_e \Phi_A}, \tag{1.10}$$

giving the dimensionless parameters

$$l = \frac{L}{H}, \quad d = \frac{D}{H}, \quad k = KH, \quad \kappa_{be} = \frac{\kappa_b}{\kappa_e}. \tag{1.11}$$

Substitution of Eqs. (1.10) and (1.11) in the system of dimensional Eqs. (1.1)–(1.9) results in the system of dimensionless equations

$$\nabla^2 \phi_e(x, y) = 0, \tag{1.12}$$

$$\nabla^2 \phi_b(x, y) = 0, \tag{1.13}$$

$$\phi_e(x, 1) = \sin(kx),$$
$$\phi_e(x, d) = \phi_b(x, d),$$
$$\left[-\kappa_e \frac{\partial \phi_e}{\partial y}\right]_{x, y = d} = \left[-\kappa_b \frac{\partial \phi_b}{\partial y}\right]_{x, y = d}, \tag{1.14}$$
$$\left[\frac{\partial \phi_b}{\partial y}\right]_{x, y = 0} = 0.$$

This system has a simple analytical solution

$$\phi_e = \frac{\sin(kx) e^{k(-1+2d-2y)} [C_1(e^{-k(-3y+2d)} + e^{-k(2d-y)}) + C_2(e^{-k(4d-3y)} + e^{ky})]}{C_1(e^{-2k} + 1) + C_2(e^{2k(-1+d)} + e^{-2kd})}, \tag{1.15}$$

$$\phi_b = \frac{2\sin(kx)[e^{2ky}+1]e^{-k(1+y)}}{C_1(e^{-2k}+1)+C_2(e^{2k(-1+d)}+e^{-2kd})}, \quad (1.16)$$

where $C_1 = \kappa_{be} + 1$ and $C_2 = 1 - \kappa_{be}$. For the current in the electrolyte,

$$\bar{i}_e(x, y) = -\nabla\phi_e, \quad 0 \le x \le l, \quad d \le y \le 1 \quad (1.17)$$

and in the steel band,

$$\bar{i}_b(x, y) = -\kappa_{be}\nabla\phi_b, \quad 0 \le x \le l, \quad 0 \le y \le d. \quad (1.18)$$

The algebraic expressions for $\bar{i}_e$ and $\bar{i}_b$ are shown in Appendix.

Sensitivity Analysis

The sensitivity of the current and energy efficiencies, and of the potential and current distributions to the parameters, *k* and *d* were investigated. The efficiencies of interest are defined below. The current efficiency, η_i, represents the ratio of the current entering the band and that coming out of the electrode. As seen from equations for $i_{e,y}$ and $i_{b,y}$ in Appendix, this ratio remains constant for given values of *k*, *d*, and κ_{be} at any given *x*. In a general geometry this is of course not so, but happens to be the case here due to the geometrical simplifications made. From the definition

$$\eta_i = \frac{i_{b,y}(x, y = d)}{i_{e,y}(x, y = 1)} \quad (1.19)$$

one finds that

$$\eta_i = \frac{2\kappa_{be}[e^{2kd}-1]e^{-k(-2+3d)}}{C_1(e^{-k(-3+2d)}-e^{-k(2d-1)})+C_2(e^{-k(4d-3)}-e^{k})}. \quad (1.20)$$

The electric energy transfer efficiency (from electrode to steel band), η_e, is the ratio of the energy entering the band and that leaving the electrode,

$$\eta_e = \frac{\phi_b(x, y = d)i_{b,y}(x, y = d)}{\phi_e(x, y = 1)i_{e,y}(x, y = 1)}, \quad (1.21)$$

which is thus

$$\eta_e = \frac{4\kappa_{be}[e^{2kd}-1][e^{2kd}+1]e^{-2k(-2+3d)}}{[C_1(e^{-2k(-2+3d)}-e^{-k(2d-1)})+C_2(e^{-k(4d-3)}-e^{k})][C_1C_3+C_2C_4]}, \quad (1.22)$$

where $C_3 = e^{-k(-3+2d)}$ and $C_4 = e^{-k(4d-3)} + e^{k}$.

EXPERIMENTAL

The experimental cell (Fig. 3) is composed of a 360 by 260 by 235 mm rectangular glass tank (*1*) containing a solution of neutral sodium sulfate (*7*); two magnetic stirrers in the bottom of the cell, which could be used to stir the solution when desiring to get electrolyte motion; an electrode assembly consisting of two sets of electrodes, with three lead anodes (*2*) and three stainless steel cathodes (*3*), placed symmetrically above and below a stationary steel band; a regulated 1-kW dc power supply; a 1–10 V (±0.5% + 1 dgt.) voltmeter; and a 1–10 A (±1.5% + 5 dgts.) ammeter. Type 316 stainless steel bands (*5*), 50 by 3 by 300 mm were used. Some of them were pickled before the experiment at the Avesta Sheffield AB annealing and pickling line and some were not, the latter having attained oxide scale on the surface during the annealing. The band was stationary, supported by two Plexiglas™ holders (*4*). To allow measurement of the current passing through the steel band, it was cut vertically into two equal parts. Stainless steel rods, type 304SS, ø4 mm, length 185 mm (*6*) with a resistance of 0.0012 ohm were screwed on to each of the halves. The two halves were glued end-to-end by 3 mm electrically insulating silicon cement between them. This way the current that passed through the steel strip was forced through the steel rods and through an ammeter. The cell was placed on two magnetic plates for activating the magnetic stirrers when needed. The temperature in the cell was 21 ± 1/2°C.

At first, to examine whether cutting the strip as described above would affect the results, an uncut stainless strip was used, the voltage was applied to the pickling cell electrodes, and the corresponding current was measured. It was found that there was no perceptible difference between the current passing in both cases.

Experiments were conducted at interelectrode distances (the distance between the two electrode sets) of 25, 50, and 90 mm. In each of these cases, the upper and lower electrode-to-band distances were set to 18 mm and 28 mm respectively, dictated by the size limitations of the experimental cell. The electrode setup is shown in Fig. 3. The measurement procedure was to increase the voltage from 1 to 10 V and simultaneously measure the total current through the electrodes and through the steel band. A current density of 1 kA m^{-2} was of particular interest, since it is used in actual full-size pickling facilities; 10 A was sufficient to attain the desired current density since the total area of the anodes was 100 cm^2.

RESULTS AND DISCUSSION

Potential and Current Distributions

The results from the analytical model were calculated with the following parameters that appear in the experiment $\kappa_b = 10^7$ S m^{-1}, $\kappa_e = 9.87$ S m^{-1} (for the con-

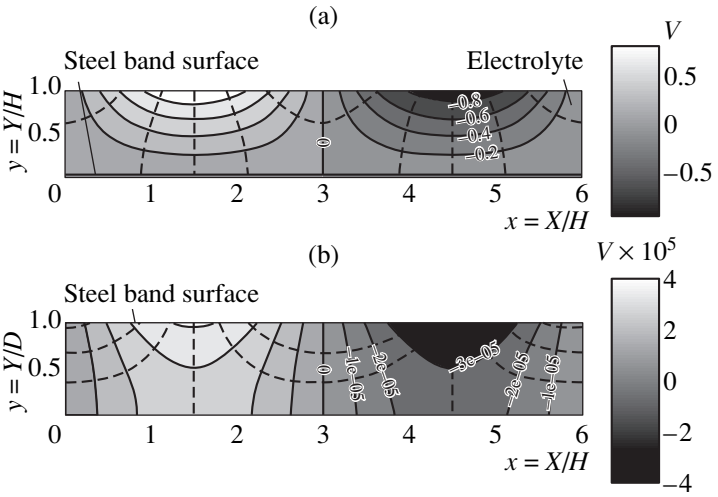

Fig. 4. Dimensionless potential and current field plots as calculated from the mathematical model for H = 50 mm, D = 1.5 mm, L = 300 mm, $c_{Na_2SO_4}$ = 170 g l^{-1}, κ_e = 9.87 S m^{-1}, and $\kappa_b = 10^7$ S m^{-1}: (a) potential field (solid lines) and current field (dashed lines) in electrolyte, and (b) potential and current fields in the steel band.

centration $c_{Na_2SO_4}$ = 170 g l^{-1}), D = 1.5 mm, the electrode-to-band distance $H - D$ = 48.5 mm and k = 20.94 m^{-1}.

Figure 4 shows the potential and current distributions predicted by the model, where it is seen that nearly all of the potential drop occurs in the electrolyte and that the potential in the steel band is 10^{-5}, i.e. nearly zero. The potential distribution in the electrolyte and the band is positive and negative, corresponding to the sign of the applied sine wave voltage simulating the electrode potential. Figure 4 also illustrates the large potential drop in the electrolyte, caused by the great difference in the electrolyte and steel band conductivities. For clarification, Fig. 4b shows a magnification of the potential and current fields in half of the steel band. The contour lines show that the potential drop in the steel band is very small, because its conductivity is relatively high compared to that of the electrolyte.

Figure 5a illustrates the direction of the current. As can be observed, much of the current passes directly from the anodes to the cathodes without entering the steel band. This is to be expected, since the current travels where it encounters the lowest resistance, and this results in a decrease in the efficiency of the process. Figure 5b shows this lost current i_{lost}

$$i_{lost} = (i_{e,y} - i_{b,y})/i_{e,y}, \qquad (1.23)$$

calculated as a function of the distance from the band for different electrode–band distances. It is obvious that i_{lost} increases with the band–electrode distance, and it is noteworthy that its increase is lowest near the band and largest in the intermediate region, with respect to the ordinate.

Figure 6 shows a comparison between the model-predicted and experimentally-measured total and band φ vs. i curves. One can see that the trends and the fact that only a fraction of the total current passes through the steel band agree qualitatively, but, as expected, the actual values do not. Since the experimental errors are within a few percent only, the large discrepancy can be explained primarily by the simplicity of the model, which, as stated in Introduction, at this stage still excludes the full complexity of the pickling process, such as the generation, presence, and motion of the bubbles and the band–surface chemical reactions.

To illustrate the effect of the bubbles, Fig. 7a shows a side-view of the steel band with oxygen and hydrogen bubbles sticking on the bottom and top surface, and Fig. 7b shows the bottom view of the anodes, with oxygen bubbles sticking and coalescing on the surface, both photos taken during the experiment. The presence of the bubbles obviously insulates parts of the band and the electrodes and reduces the conductivity of the electrolyte through which they rise. This is especially in effect on the bottom surfaces of the band and the electrode, because they are hindered from rising and may thus stay long enough to coalesce into larger ones, thereby creating more insulating layers. This is verified by our experimental observation that the bottom surface is much less pickled than the top one. Bubble-caused insulation obviously results in a less efficient pickling process.

Current and Energy Efficiencies

The current and energy efficiencies calculated as a function of a dimensionless electrode–band distance are shown in Fig. 8a. As expected, the current efficiency decreases as the electrode distance increases, due to both the increased path resistance and the increased interelectrode short-circuit current. Figure 8b is a plot of the corresponding electrode and band potential ϕ_e

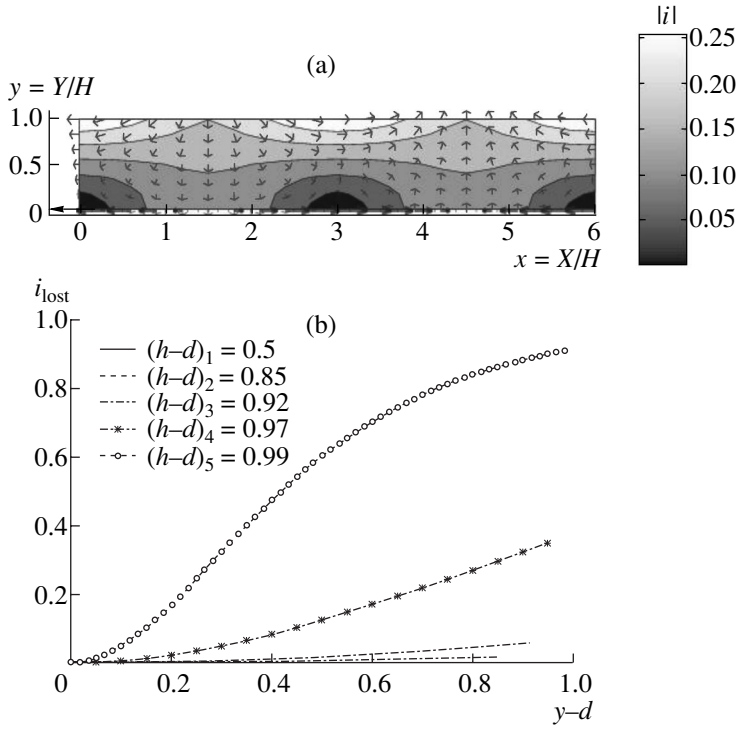

Fig. 5. (a) Dimensionless current distributions in electrolyte and band, calculated for L = 300 mm, H = 50 mm, D = 1.5 mm, κ_e = 9.87 S m^{-1}, and $\kappa_b = 10^7$ S m^{-1}; arrows indicate the current direction, and solid lines, its magnitude; and (b) current lost (i_{lost}) due to short-circuiting between electrodes, as a function of the vertical position, for different electrode-to-band distances $h - d$, where h = 1.

and ϕ_b at chosen x location (x = 1/4), since the potential is proportional to sin(kx), and corresponding current densities, as a function of the dimensionless electrode–band distance.

As expected, the efficiencies and the current and potential in the electrolyte decrease as the electrode–band distance increases. The electrode potential is imposed and is therefore obviously not affected. The decrease in the energy efficiency is at least 5 orders of magnitude larger than that of the current efficiency because of a similar drop in the potential (Fig. 8b). It is noteworthy that the energy efficiency curve has an inflection point at $(H - D)/H_{typ} \approx 0.6$. For the system analyzed here, it implies that maintaining the electrode–band distance below 18 mm, instead of the base case of 28.5 mm, would results in important improvement in efficiency.

Figure 9a displays the current and energy efficiencies as a function of a dimensionless band thickness d while the electrode–band distance is maintained constant. The current efficiency is nearly independent of d, but the energy efficiency decreases strongly as d increases. The explanation is in the fact, clarified by the dimensionless electrode and band potential and current plots in Fig. 9b, that increasing d reduces the resistance between the band surface and zero-potential center, thus bringing the band surface potential closer to zero. The electrode potential is a constant as set, and the currents remain nearly constant.

Figure 10a shows that the current efficiency and energy efficiency increase and decrease, respectively, to constant values as the conductivity ratio d increases. The explanation, reinforced by Fig. 10b, is that the electrode current increases and the band potential

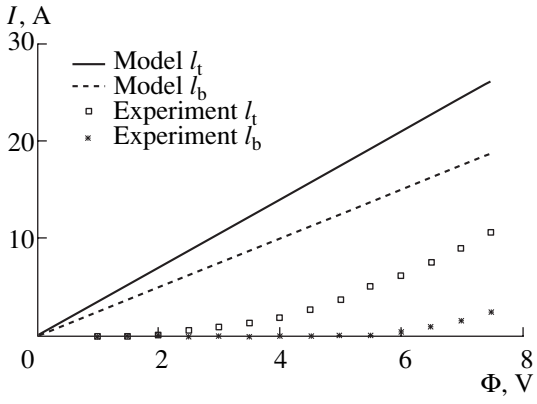

Fig. 6. Comparison between the analytical model and experimental results of the total and band current–voltage relationship; L = 300 mm, H = 20 mm, D = 1.5 mm, $c_{Na_2SO_4}$ = 170 g l^{-1}, κ_e = 9.87 S m^{-1}, $\kappa_b = 10^7$ S m^{-1}, and T = 21°C.

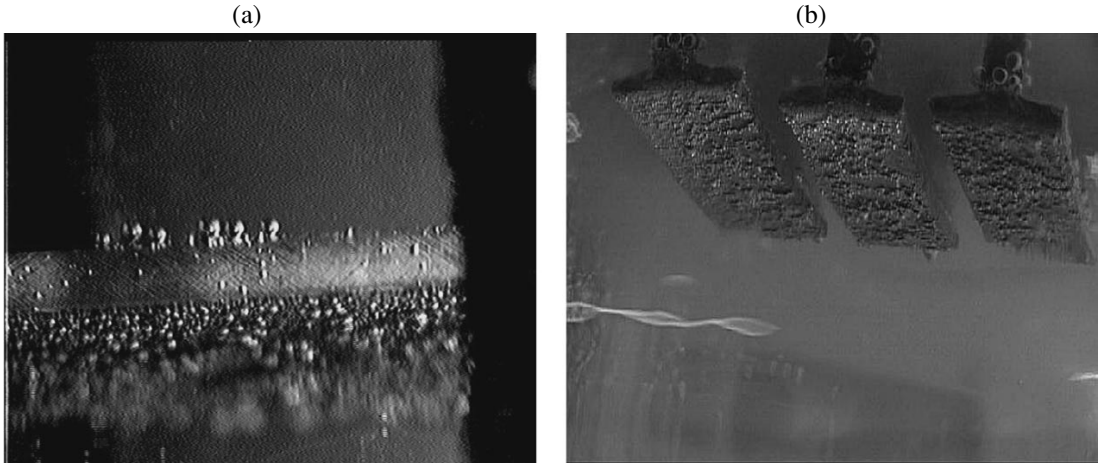

Fig. 7. Oxygen and hydrogen bubble evolution and presence on the electrodes, three minutes after the start of a pickling experiment: (a) side-view of steel band, showing oxygen and hydrogen bubbles sticking on the bottom and top surfaces; and (b) bottom view of anodes, showing oxygen bubbles sticking and coalescing on the surface; photographs taken with a CCD video camera, 8× magnification; $\Phi = 6.67$ V, $I = 1.43$ A, $T = 21$°C.

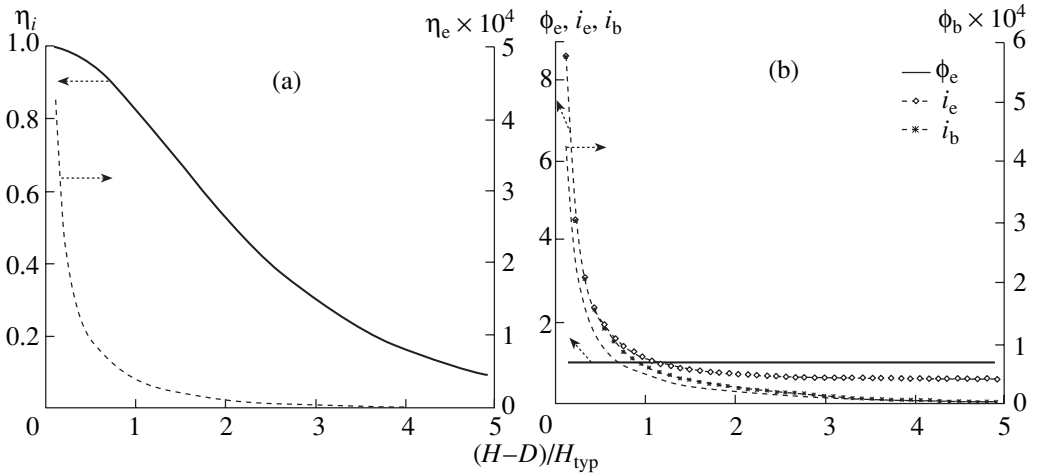

Fig. 8. (a) Current (η_i) and energy (η_e) efficiency plots as a function of electrode-to-band distance $(H - D)/H_{typ}$; $D = 1.5$ mm, $H_{typ} = 30$ mm, $L = 300$ mm, $\kappa_e = 9.87$ S m^{-1}, and $\kappa_b = 10^7$ S m^{-1}; and (b) dependence of dimensionless electrode and band potentials $\phi_e(x = l/4)$ and $\phi_b(x = l/4)$ and corresponding current densities $i_e(x = l/4)$ and $i_b(x = l/4)$ on $(H - D)/H_{typ}$.

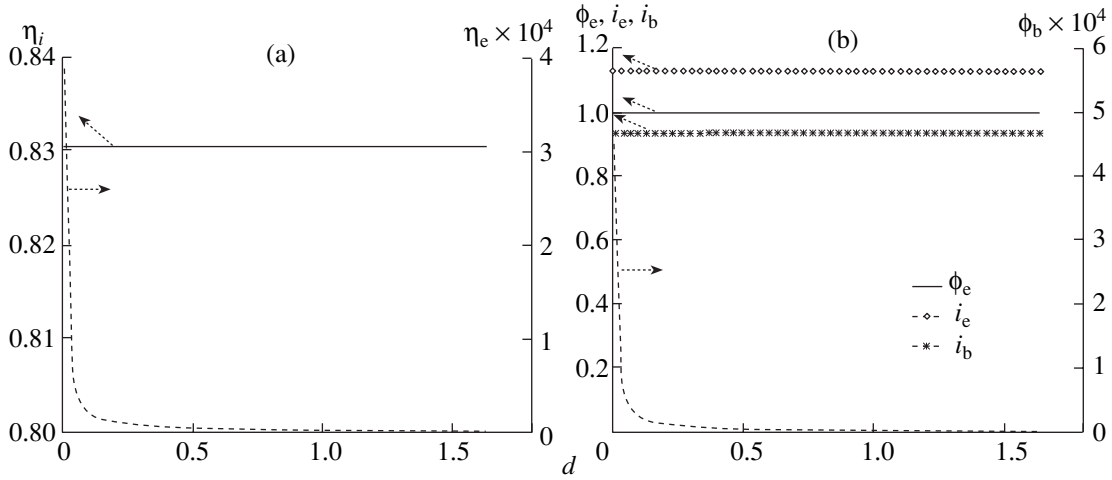

Fig. 9. (a) Current (η_i) and energy (η_e) efficiency dependence on half-band thickness d at $h = 1$ and $(H - D)$ constant, $L = 300$ mm, $\kappa_e = 9.87$ S m^{-1}, and $\kappa_b = 10^7$ S m^{-1}; and (b) dependence of dimensionless potentials $\phi_e(x = l/4)$ and $\phi_b(x = l/4)$ and corresponding current densities $i_e(x = l/4)$ and $i_b(x = l/4)$ on d.

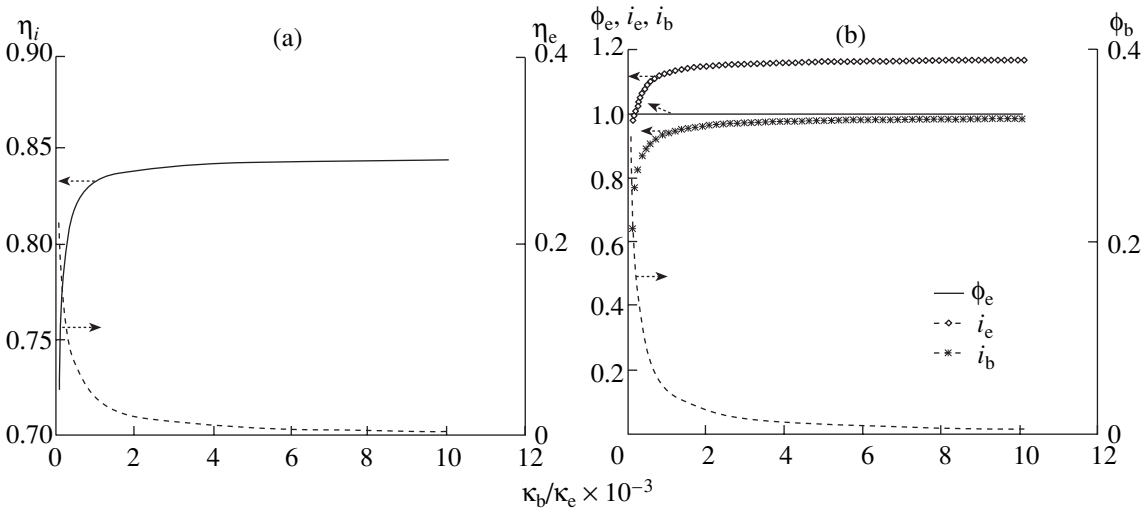

Fig. 10. Dependence of (a) current (η_i) and energy (η_e) efficiencies on the electrolyte-to-band conductivity ratio κ_b/κ_e at $h = 1$ and $H - D$ constant, $d = 0.05$, $L = 300$ mm; and (b) dependence of dimensionless potentials $\phi_e(x = l/4)$ and $\phi_b(x = l/4)$ and corresponding current densities $i_e(x = l/4)$ and $i_b(x = l/4)$ on κ_b/κ_e.

decreases (but much more significantly) due to the resistance decrease occurring by either the decrease in the electrolyte conductivity (lower concentration) or by the increase in the band conductivity. The asymptotic values of the efficiencies are due to specific geometric configuration of the system chosen for this analysis.

CONCLUSIONS

The experimental work has demonstrated a strong bubble production and a significant adherence to the surfaces, the latter especially at the bottom surfaces of the band and electrodes, and its effects on reducing pickling efficiency and creating unevenly pickled steel surfaces. The pickling efficiency is about 30%, confirming other researchers' results.

The analytical model developed and evaluated here shows trends very similar to those observed in the experiments, but naturally does not agree, nor was it expected to agree, with those quantitatively, because it ignores bubble generation, chemical reactions, and flow. Nevertheless, it provides very valuable guidance. First, it shows that the current efficiency decreases as the electrode–band distance increases, and it increases with the band thickness d and the band-to-electrolyte conductivity ratio. The energy efficiency decreases by orders of magnitude faster with all of the above-mentioned parameters, because of the correspondingly strong drop in the band–surface potential. Second, it reveals that a large amount of current is lost, i.e. not imposed onto the band, due to interelectrode short-circuiting. This loss can be reduced by decreasing the electrode–band distance.

In future work, the modeling will include the bubble evolution, the chemical reactions, and the turbulent fluid flow present during the pickling process.

ACKNOWLEDGMENTS

This work has been conducted at the Faxen Laboratory of the Royal Institute of Technology (KTH). We gratefully acknowledge the advise and help given by Dr. Michael Vynnyncky, Dr. Göran Lindbergh, and the financial support by Avesta Shelfield AB.

NOMENCLATURE

$c_{Na_2SO_4}$—electrolyte concentration, g l^{-1}

d—dimensionless half thickness of steel band, D/H

D—half thickness of steel band, m

H—distance between electrodes and steel band center-line, m

K—dimensional periodicity of the sine wave function, m

L—steel-band length, m

l—dimensionless steel-band length, L/H

$\bar{I}_{e,b}$—current density vector, A m^{-2}

$\bar{i}_{e,b}$—dimensionless current density vector, $\dfrac{HI_{e,b}}{\kappa_e \Phi_A}$

$i_{e,x}$—x-vector of dimensionless electrolyte current i_e

$i_{e,y}$—y-vector of dimensionless electrolyte current i_e

$i_{b,x}$—x-vector of dimensionless electrolyte current i_b

$i_{b,y}$—y-vector of dimensionless electrolyte current i_b

$i_{conserv}$—sum of the current in a half cell of the model

$|I|$—magnitude of dimensionless current, $\sqrt{i_x^2 + i_y^2}$

I—total current measured in experiment, A

i_{lost}—lost current passing directly between electrodes, $(i_{e,y} - i_{b,y})/i_{e,y}$

k—dimensionless periodicity in the x-direction, kH
n—number of sine waves
n_x—x-component of normal vector
n_y—y-component of normal vector
X—distance measured along steel-band surface, m
Y—normal distance from steel-band surface, m
x—dimensionless distance measured along the steel band surface, X/H
y—dimensionless normal distance from the surface, Y/H

GREEK SYMBOLS

η_i—current efficiency
η_e—energy transfer efficiency
κ_e—conductivity of electrolyte, S m^{-1}
κ_b—conductivity of steel band, S m^{-1}
κ_{be}—dimensionless conductivity ratio, $\dfrac{\kappa_b}{\kappa_e}$
Φ_A—electrode potential amplitude, V
Φ_e—electrode potential, V
Φ_b—steel-band potential, V
ϕ_e—dimensionless potential of electrolyte
ϕ_b—dimensionless potential of steel band

SUBSCRIPTS REFER TO

$(\ldots)_A$ imposed electrode voltage
$(\ldots)_b$ steel band
$(\ldots)_e$ electrolyte
$(\ldots)_i$ dimensionless current
$(\ldots)_E$ dimensionless energy
$(\ldots)_X$ dimensional X direction
$(\ldots)_Y$ dimensional Y direction
$(\ldots)_x$ dimensionless X direction
$(\ldots)_y$ dimensionless Y direction

APPENDIX

Algebraic Expressions

The algebraic expressions for the current in the electrolyte, $\bar{i}_e$

$$i_{e,y} = \frac{-k\sin(kx)e^{k(-1+2d-2y)}[C_1(-e^{-k(-3y+2d)} + e^{-k(2d-y)}) + C_2(-e^{-k(4d-3y)} + e^{ky})]}{C_1(e^{-2k}+1) + C_2(e^{2k(-1+d)} + e^{-2kd})}$$

$$i_{e,x} = \frac{-k\cos(kx)e^{k(-1+2d-2y)}[C_1(e^{-k(-3y+2d)} + e^{-k(2d-y)}) + C_2(e^{-k(4d-3y)} + e^{ky})]}{C_1(e^{-2k}+1) + C_2(e^{2k(-1+d)} + e^{-2kd})}$$

Similarly, the current in the steel band is

$$i_{b,y} = \frac{-2\kappa_{be}\sin(kx)k[e^{2ky}-1]e^{-k(1+y)}}{C_1(e^{-2k}+1) + C_2(e^{2k(-1+d)} + e^{-2kd})},$$

$$i_{b,x} = \frac{-2\kappa_b\cos(kx)k[e^{2ky}+1]e^{-k(1+ky)}}{C_1(e^{-2k}+1) + C_2(e^{2k(-1+d)} + e^{-2kd})},$$

where $C_1 = \kappa_{be}$ and $C_2 = 1 - \kappa_{be}$.

REFERENCES

1. *Sheet Met. Ind.*, 1979, vol. 56, pp. 36, 39, 40, 42.
2. Covino, B.S., *Electrochim. Acta*, 1960, vol. 3, p. 233.
3. Braun, E., *Iron Steel Eng.*, 1980, vol. 57, p. 79.
4. Hudson, R.M., in *ASM Handbook*, vol. 5: *Surface Engineering*, ASM Intl. (USA), 1994, p. 67.
5. Dunaevskii, V.I., Stepanenko, V.T., Shnol, M.Ya., and Vespalko, L.N., *Protection of Met.*, 1985, vol. 21, p. 359.
6. Shapovalov, E.T., Kazakova, G.V., and Andrushova, N.V., *Steel USSR*, 1983, vol. 13, p. 27.